dynardo
dynamic software & engineering

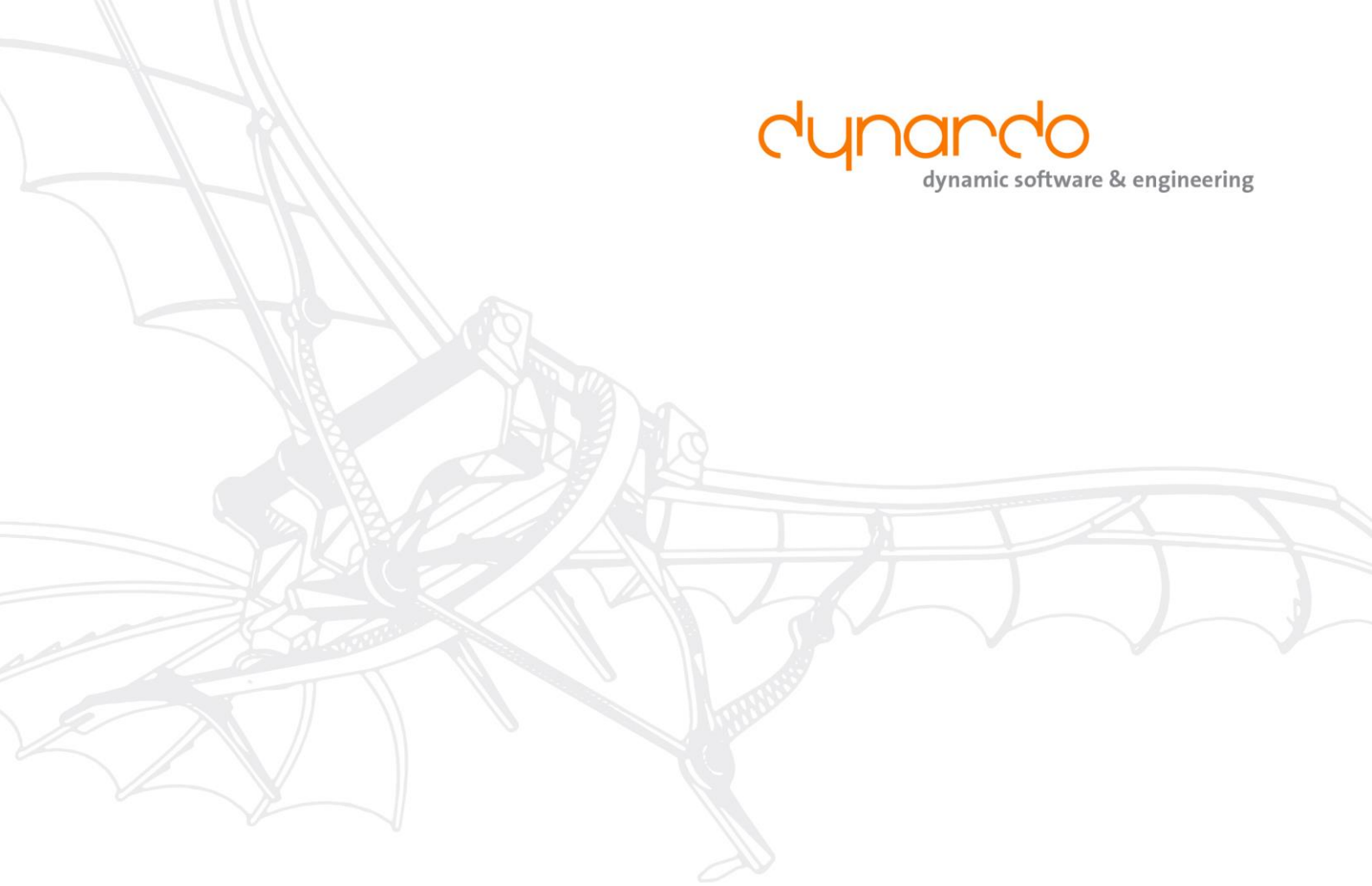

Lectures

Simulation of Penny Shaped Fracture using homogenized continuum approach

S. Venkat, St. Eckardt, J. Will

presented at the Weimar Optimization and Stochastic Days 2015
Source: www.dynardo.de/en/library

Simulation of Penny Shaped Fracture using homogenized continuum approach

Swami S. Venkat, Stefan Eckardt and Johannes Will

Dynardo GmbH

Abstract

In this paper, the propagation of hydraulically driven fracture in a fully saturated low permeable medium using the homogenized continuum approach is compared to theoretical solution, as well as to solutions using discrete joint modelling with cohesive zone elements and XFEM.

As the unconventional reservoirs consist of low permeable jointed rocks, the fracture generation and the fluid flow is largely influenced by stress and strength anisotropies, resulting from naturally occurring in situ joints. Therefore, 3D modelling is essential, since the prediction of fracture growth in 3D is the key to investigating different fracture designs and furthermore different operational parameters in order to optimize the oil and gas production from unconventional reservoirs.

To show the ability of the homogenized continuum approach to represent theoretical solutions, the simulation results obtained with this approach is compared with the asymptotic analytical solutions obtained for Penny-shaped models in the toughness/storage propagation regimes. The results based on the homogenized continuum approach to represent the fracture growth are also compared to the discrete fracture modelling in continuum mechanics using cohesive zone elements and XFEM which are discussed in [1].

Keywords: Unconventional shale oil and gas Reservoirs, Jointed Rocks, Geomechanics, Homogenized Continuum Approach, Hydraulic Fracturing simulation

1 Introduction

Large amount of unconventional gas and oil is produced from shale reservoirs. Hydraulic fracturing is the process of stimulating these low permeable shale rocks to increase their permeability for the production of oil and gas. In any given hydraulic fracturing venture its economics depends to a large extent on the operational conditions which comprise for example the number of wells drilled, slurry injection rates or wellbore pressures etc. These operational conditions along with the intrinsic reservoir parameters determine the fracture network dimensions (length/height/width) and geometry which are essential to ascertain the oil or gas production.

In unconventional reservoirs, being low permeable jointed rocks, the fracture generation and the fluid flow is largely influenced by stress and strength anisotropies, resulting from naturally occurring in situ joints or the planes of weaknesses. Therefore, 3D modelling of the fracture growth is essential to investigating the different fracture designs and furthermore different operational parameters in order to optimize the oil and gas production from unconventional reservoirs [2].

Dynardo has developed during the last 15 years a hydraulic fracturing simulation environment based on ANSYS® implicit finite element code for parametric FEM modeling, b) Dynardo's material modelling environment multiPlas® for material modeling of naturally fractured shale rocks and c) Dynardo's toolbox for parametric variation optiSLang® for sensitivity analysis and calibration of large number of reservoir parameter as well as engineering and operational conditions parameters and their influence on the final stimulated rock volume and the uplift potentials. Since 2008 the hydraulic fracturing simulation environment has successfully been applied to unconventional oil and gas reservoirs world-wide [3].

Unlike the vast majority of commercial and scientific approaches which use the discrete modelling technique, the Dynardo approach on the other hand is based on a homogenized continuum approach to simulate the hydraulic fracturing process in the jointed shale rocks without being forced to predefine possible fracture locations.

The main motivation of choosing the homogenized continuum approach is that it is numerically much more efficient for running the 3-D coupled hydraulic-mechanical simulations of hydraulic fracturing process in comparison to other alternatives investigated today like discrete joint modelling, XFEM or particle methods.

Starting from the scientific framework of modelling water flow in jointed rock using the homogenized continuum approach in the field of rock mechanics and dam engineering [4] Dynardo has improved and enhanced that approach for unconventional hydrocarbon applications, nuclear waste disposal applications [5] or Enhanced Geothermal System (EGS) applications. In addition to the base work of Wittke and others [4], the approach was generalized for coupled hydraulic-mechanical simulation of jointed rocks using theory of consistent integration of multi-surface plasticity which was mandatory to deal numerically consistent and effective with multiple sets of joints and matrix rock in the homogenized continuum approach. These developments provide the basis for the Dynardo library of constitutive material models multiPlas, which has been continuously improved and verified with different geomechanic applications in the last 20 years.

In this paper the chapter 2 covers the governing equations for multi-surface plasticity and the hydraulic model used in the Dynardo fracturing simulator. The chapter 3 constitutes the fracture propagation regimes, the model setup along with mesh, boundary conditions and the parameter description including a sensitivity and optimization study to calibrate parameters. Chapters 4 and 5 present the results and conclusion\future work respectively.

2 Physical phenomena and governing Equations

The hydraulic fracturing simulator for the 3-dimensional simulation of the hydraulic fracturing process is based on coupled hydraulic-mechanical finite element analysis as shown in *Fig. 1*.

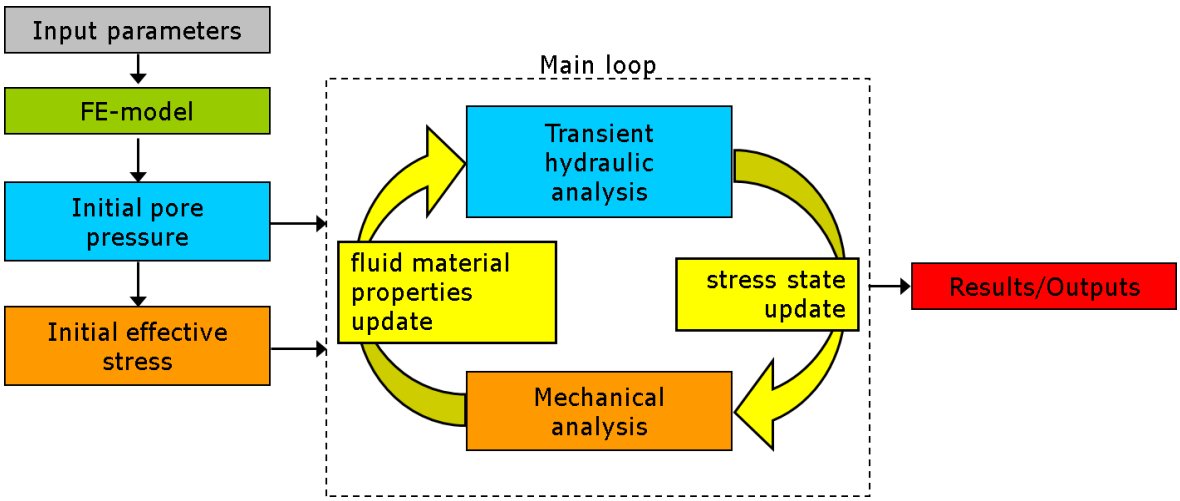

Fig. 1 The Dynardo coupled hydraulic-mechanical fracturing simulator

The main features of the fracturing simulator are as listed below:

i. Non-linear mechanical analysis using multi-surface plasticity for modelling fracture network activation in jointed rocks within homogenized continuum approach.
ii. Hydraulic model is based on the assumption of laminar flow in multiple parallel joint systems.
iii. The mechanical to hydraulic coupling which involves computation of fracture opening and closure resulting in anisotropic hydraulic jointed rock conductivity.
iv. The hydraulic to mechanical coupling which involves computation of flow forces which depends on the pressure gradients within the jointed rock.
v. Very important to realistically simulate the non-linear history of fracture network creation and activation is the initialization of reservoir conditions, the initial in situ strength, stress and pore pressure conditions.

2.1 Non-Linear Mechanical Analysis

The jointed rock is modelled using the homogenized continuum approach. These rocks are modelled within the strength definition in the mechanical domain as volume consisting of matrix material (intact rock) and up to 6 strength anisotropies (joints), which represent in situ joint systems as well as new joints created by intact rock failure. For the material modelling multiPlas [6] is used, which consists of elastic-plastic algorithms including damage and residual strength for efficient numerical handling multi surface plasticity as a result of multiple possible failure mechanisms of tensile and shear failure of matrix rock and every site joint sets.

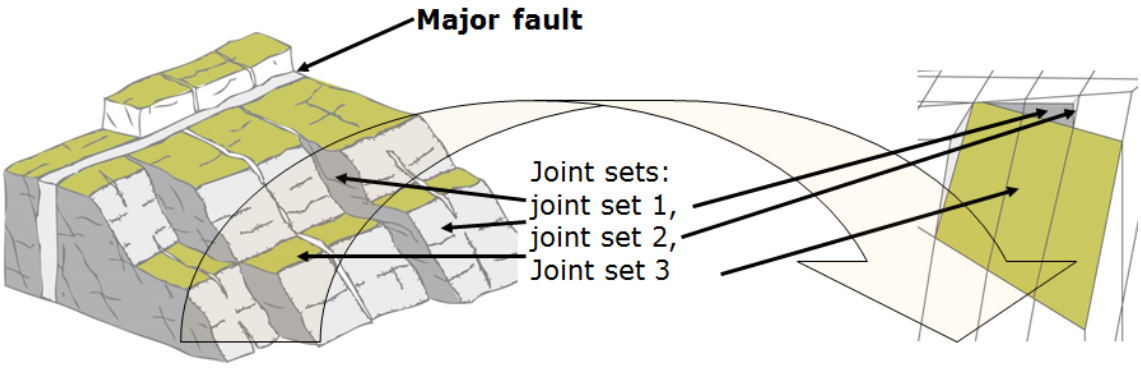

Fig. 2 The joint sets or the planes of weaknesses in the shale rocks.

In the hydraulic fracturing simulator the strength conditions of jointed rock are modelled using a combination of isotropic Mohr-Coulomb and Rankine yield surface for the intact rock and anisotropic Mohr-Coulomb and tension cut-off yield surfaces. The isotropic Mohr-Coulomb yield surface is as shown in the *Fig. 3* below. In the general three-dimensional stress space, the Mohr-Coulomb yield criterion is defined as follows:

$$F_{MC} = \sigma_m \sin\varphi + \sigma_s \left(\cos\theta - \frac{\sin\theta \sin\varphi}{\sqrt{3}} \right) - c\cos\varphi = 0 \tag{1}$$

with

$$\sigma_m = \frac{\sigma_x + \sigma_y + \sigma_z}{3} \tag{2}$$

$$\sigma_s = \sqrt{J_2} \tag{3}$$

$$\sin(3\theta) = \frac{3\sqrt{3}}{2} \frac{J_3}{\sqrt{J_2^3}} \tag{4}$$

where σ_m is the hydrostatic stress, J_2 and J_3 are second and third invariant of the deviatoric stress tensor, θ is the so-called Lode angle, φ is the friction angle and c is the cohesion. In the special cases of $\varphi = 0°$ and $\varphi = 90°$ the Mohr-Coulomb yield surface reduces to the Tresca yield surface and the Rankine criterion respectively. A non-associated flow rule is considered with the plastic potential,

$$Q_{MC} = \sigma_m \sin\psi + \sigma_s \left(\cos\theta - \frac{\sin\theta \sin\psi}{\sqrt{3}} \right) \tag{5}$$

where ψ is dilatancy angle. With the Mohr-Coulomb yield criterion the uniaxial compressive strength f_c and uniaxial tensile strength f_t are functions of friction angle and cohesion.

$$f_c = c\frac{2\cos\varphi}{1-\sin\varphi} = 2c\tan\left(45 + \frac{\varphi}{2}\right) \tag{6}$$

$$f_t = c\frac{2\cos\varphi}{1+\sin\varphi} = 2c\tan\left(45 - \frac{\varphi}{2}\right) \tag{7}$$

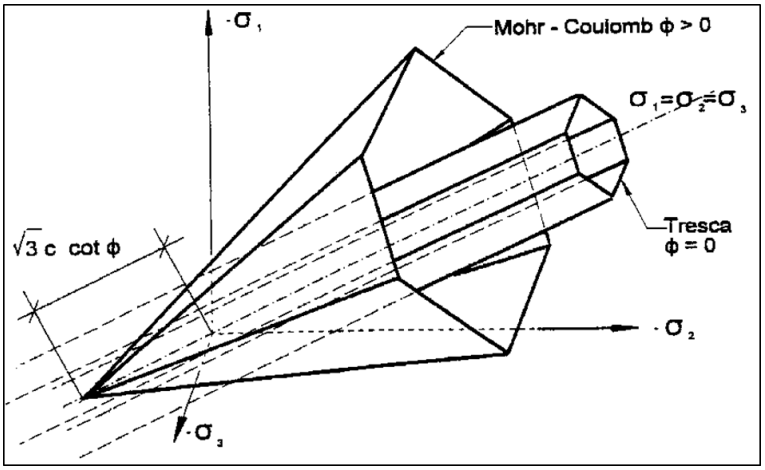

Fig. 3 The isotropic Mohr-Coulomb yield surface [6].

The Mohr-Coulomb yield surface in general overestimates the uniaxial tensile strength which is very low for jointed rocks and that being the reason for it to be combined with the tension cut-off or Rankine yield surface. The Rankine yield function is given by the equation below.

$$F_{RK} = \sigma_m + \frac{2}{\sqrt{3}}\sigma_s \sin\left(\theta + \frac{2}{\sqrt{3}}\pi\right) - f_t = 0 \tag{8}$$

where f_t is the tensile strength. For the Rankine yield surface an associated flow rule is assumed. Note that the Rankine yield surface can be disabled by setting

$$f_t \geq \frac{c}{\tan\varphi} \tag{9}$$

The anisotropic Mohr-Coulomb yield surface describes the material behavior of the joint sets within the jointed rocks. Consequently, at every joint surface the general three-dimensional stress space is reduced to a stress component normal to the plane and two stress components tangential to the plane. *Fig. 4* shows the Mohr-Coulomb yield surface in terms of the normal joint stress and the tangential joint stress. Furthermore, the yield surface additionally becomes a function of the plane orientation which is represented by two orientation angles α and β. *Fig. 5* illustrates the definition of the orientation angles.

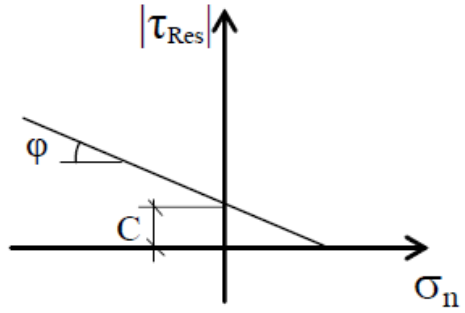

Fig. 4 The anisotropic Mohr-Coulomb yield surface [6].

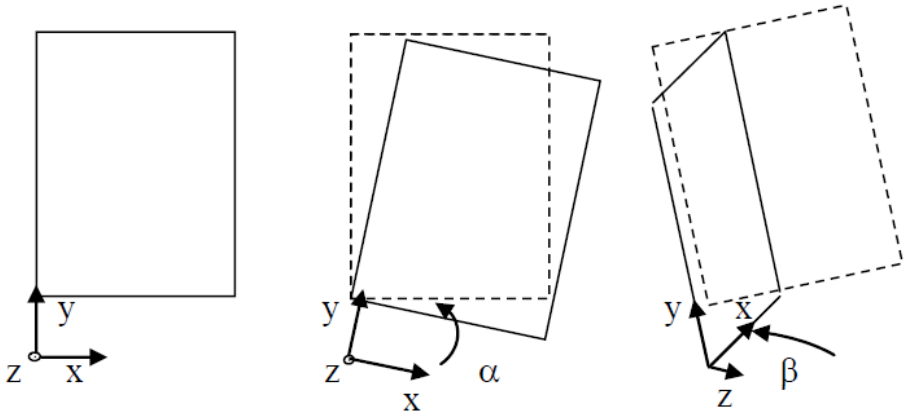

Fig. 5 The orientation angles definition of joint sets [6].

These orientation angles α and β are respectively the rotation against positive rotational direction about the z axis and rotation in positive rotational direction about the y-axis. Physically these angles represent the joint orientations, strike angle (α) and dip magnitude (β)

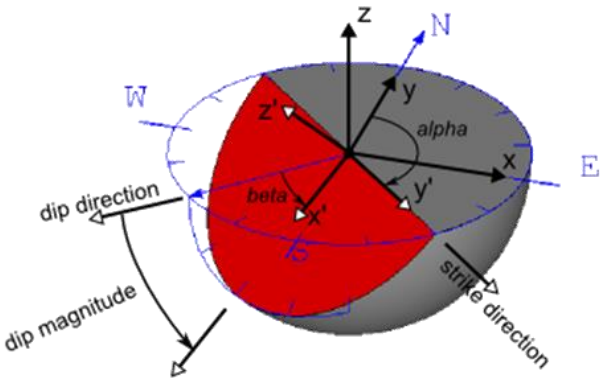

Fig. 6 The orientation angles: dip magnitude and strike angle of a joint set [6].

The anisotropic Mohr-Coulomb yield function is given by

$$F_{MC,J} = |\tau_{Res}| - \sigma_n \tan\varphi - c = 0 \qquad (10)$$

where τ_{Res} is the shear stress in the joint and σ_n is the normal joint stress (perpendicular to the joint), φ is the friction angle and c is the cohesion. Again, a non-associative flow rule is assumed for the anisotropic Mohr-Coulomb yield surface and the plastic potential is defined as

$$Q_{MC,J} = |\tau_{Res}| - \sigma_n \tan\psi \tag{11}$$

where ψ is dilatancy angle. Similar to the isotropic Mohr-Coulomb yield surface, the tensile strength is overestimated by the anisotropic Mohr-Coulomb yield surface. Hence a more realistic description is achieved by combining it with tension cut-off yield surface, which is defined by following expression

$$F_{T,J} = \sigma_n - f_t = 0 \tag{12}$$

where f_t is the tensile strength. An associative flow rule is assumed for the Rankine yield surface. The Rankine yield surface can be disabled by setting

$$f_t \geq \frac{c}{\tan\varphi} \tag{13}$$

The material models in multiPlas offers various post yield softening functions, but in the hydraulic fracturing simulations usually a simple post-yield brittle behavior is considered owing that the uncertainty of in situ joint strength parameter is large and simplified models with a minimum number of strength parameter are preferred for the reservoir calibration process. Due to brittle post-yield behaviour, the initial strength values are reduced to the residual strength values after failure combined with elasto-plastic behavior. The multiPlas material model used in the hydraulic fracturing simulator is characterized by following parameters for the intact rock and each of the joint sets.

φ – Initial inner friction angle

φ^* – Residual inner friction angle

c – Initial cohesion

c^* – Residual cohesion

ψ – Dilatancy angle

f_t – Initial tensile strength

f^* – Residual tensile strength

In addition the following orientation angles have to be defined for each joint set.

α – Strike angle

β – Dip magnitude

2.2 Hydraulic Model

Hydraulic model is based on assumption of laminar flow in multiple joint sets within an homogenization approach. The fluid flow is predominantly laminar in nature in the joints. Darcy's law is used, which is a phenomenological description of the flow of fluid through a jointed rock. Darcy's law along with the flow equation (equation of conservation of mass) results in transient seepage equation.

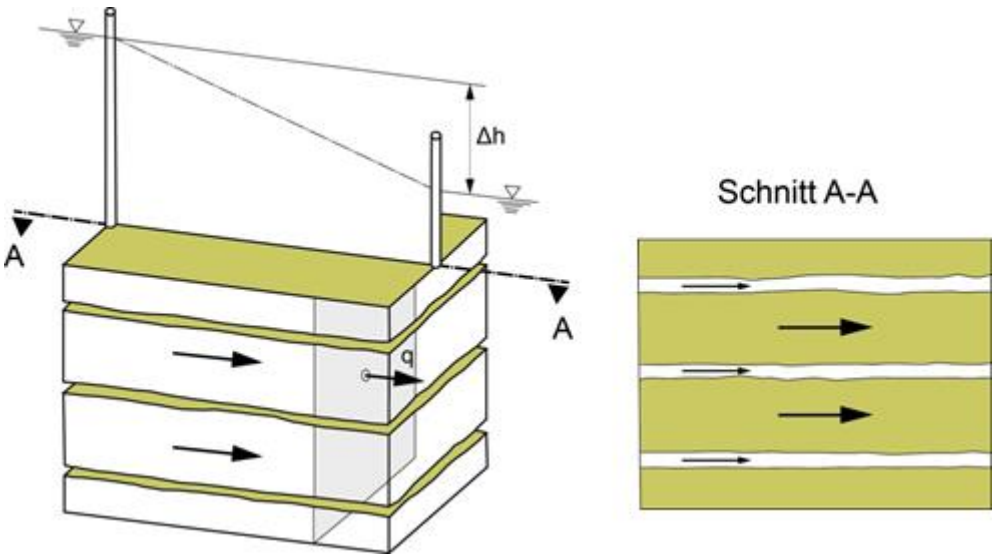

Fig. 7 Laminar fluid flow in one joint set with multiple activated joints

flow equation (mass balance): $-\nabla.\mathrm{q}+R=S_S\dfrac{\partial h}{\partial t}$ (14)

Darcy's law (momentum balance): $\mathrm{q}=-\mathrm{K}.\nabla h$ (15)

Transient seepage equation (flow equation):

$$\frac{\partial}{\partial x}\left(K_{xx}\frac{\partial h}{\partial x}\right)+\frac{\partial}{\partial y}\left(K_{yy}\frac{\partial h}{\partial y}\right)+\frac{\partial}{\partial z}\left(K_{zz}\frac{\partial h}{\partial z}\right)+R=S_S\frac{\partial h}{\partial t} \quad (16)$$

where,

h – Hydraulic height

R – General source or sink term (volume of water injected per unit volume per unit time)

K – Hydraulic conductivity

S_s – Specific storage

q – Flux vector (Darcy's velocity)

K – Hydraulic conductivity vector

The resulting transient seepage equation is solved using the finite element method.

A challenge in modelling the hydraulic part is the anisotropic conductivity of the jointed rock which is due to the combination of the following:

- The transversely isotropic hydraulic conductivity matrix of the in situ reservoir rock. In the global coordinate system this matrix is diagonal as shown below.

$$\mathrm{K_R} = \begin{bmatrix} k_{Rh} & 0 & 0 \\ 0 & k_{Rh} & 0 \\ 0 & 0 & k_{Rv} \end{bmatrix} \tag{17}$$

- The transversely isotropic hydraulic conductivity matrix of up to six joint sets, which is diagonal for a given joint in its individual joint coordinate system, but anisotropic and non-diagonal in the global coordinate system.

$$\mathrm{K}_{J,local} = \begin{bmatrix} k_J & 0 & 0 \\ 0 & k_J & 0 \\ 0 & 0 & 0 \end{bmatrix} \tag{18}$$

$$\text{and, } \mathrm{K}_{J,global} = k_J \begin{bmatrix} 1-\cos^2\alpha\sin^2\alpha & \cos\alpha\sin\alpha\sin^2\beta & -\cos\alpha\cos\beta\sin\beta \\ \cos\alpha\sin\alpha\sin^2\beta & 1-\sin^2\alpha\sin^2\beta & \sin\alpha\cos\beta\sin\beta \\ -\cos\alpha\cos\beta\sin\beta & \sin\alpha\cos\beta\sin\beta & \sin^2\beta \end{bmatrix} \tag{19}$$

The anisotropic conductivity matrix of the jointed rock can be derived by rotating the individual joint conductivity matrices in their respective local coordinate systems into the global coordinate system and then assembling them.

Total hydraulic = Intact hydraulic + Joint 1 hydraulic + Joint 2 hydraulic

$$\begin{bmatrix} k_{xx} & k_{xy} & k_{xz} \\ k_{xy} & k_{yy} & k_{yz} \\ k_{xz} & k_{yz} & k_{zz} \end{bmatrix} = \begin{bmatrix} k_{Rh} & 0 & 0 \\ 0 & k_{Rh} & 0 \\ 0 & 0 & k_{Rv} \end{bmatrix} + \begin{bmatrix} k_{J1} & 0 & 0 \\ 0 & k_{J1} & 0 \\ 0 & 0 & 0 \end{bmatrix} + \begin{bmatrix} k_{J2} & 0 & 0 \\ 0 & k_{J2} & 0 \\ 0 & 0 & 0 \end{bmatrix} + ..\text{so on} \qquad (20)$$

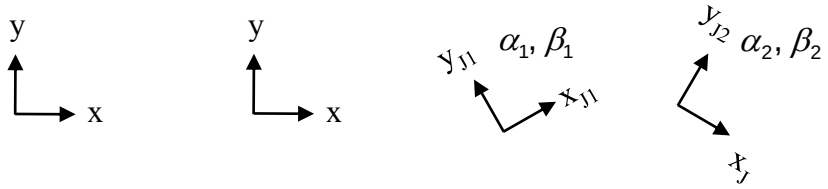

To represent anisotropic conductivity matrix, there was an anisotropic finite element for fluid flow developed, which is used for solving the transient flow equation. Following are few features of this user-element using the ANSYS user-defined element API (USER 100):

- It is an 8 node, isoparametric brick element.
- It has one degree of freedom per node, the hydraulic height
- It is a fully integrated element (2x2x2 Gauss quadrature)
- As stated above it can handle anisotropic hydraulic conductivity of jointed rocks.
- It can also support lumped storativity matrix.
- It supports element body load i.e. internal flow generation rate.

2.3 Mechanical to Hydraulic Coupling

In mechanical analysis the non-linear material behavior in every element is described at the individual points called the integration or Gauss points. For the mechanical analysis the SOLID185 element is used which is full integration element with eight integration points as shown below and each integration point represents the material behavior in the vicinity of this point in an average sense i.e. a domain is associated with each integration point.

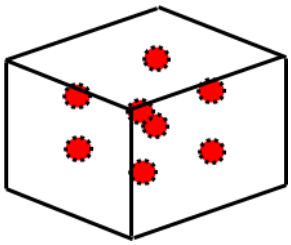

Fig. 8 SOLID185 structural solid element in ANSYS with full integration formulation (8 integration points)

The one dimensional measure of the size of this domain is the equivalent element length which is the average distance between the integration points as defined below.

$$l_{eq} = \sqrt[3]{V_e/8} \tag{21}$$

where l_{eq} is the equivalent element length of the solid 8-node element with 8 integration points and V_e is the volume of this solid element.

In the continuum approach the frequency of joint sets is defined by a parameter called the activated joint distance S for each of the joint sets. For energy preservation in the continuum approach to be valid the activated joint distance parameter for every element needs to be limited or equal to the equivalent element length. The text below will discuss that joint opening depends on the activated joint distance parameter which in turn determines the hydraulic conductivity build up in the joint sets (mechanical-hydraulic coupling).

$$S \le l_{eq} \tag{22}$$

The hydraulic conductivity tensors in the hydraulic model are coupled to plastic strain and stresses in the mechanical model. It was discussed earlier that initially without any plasticity in the model the hydraulic conductivity of the rock matrix is transversely isotropic

$$\mathrm{K_R} = \begin{bmatrix} k_{Rh} & 0 & 0 \\ 0 & k_{Rh} & 0 \\ 0 & 0 & k_{Rv} \end{bmatrix} \tag{17}$$

But upon the onset of plasticity the hydraulic conductivity tensor depends on the conductivities of plastic joint sets and also the intact rock if it attains plasticity. Hence, the global conductivity tensor K is defined as follows:

$$\mathrm{K}\left(\varepsilon^{pl},\sigma\right) = \mathrm{K}_{ini} + \sum_{i=1}^{4} \mathrm{K}_j^{(i)}\left(\varepsilon^{pl},\sigma\right) + \sum_{j=1}^{3} \mathrm{K}_I^{(j)}\left(\varepsilon^{pl},\sigma\right) \tag{23}$$

where K_{ini} is the initial hydraulic conductivity of the non-plastic rock as described in the

$$\mathrm{K_R} = \begin{bmatrix} k_{Rh} & 0 & 0 \\ 0 & k_{Rh} & 0 \\ 0 & 0 & k_{Rv} \end{bmatrix} \tag{17}.$$

The $\mathrm{K}_j^{(i)}\left(\varepsilon^{pl},\sigma\right)$ is the global hydraulic conductivity tensor of activated joints sets as shown in

eqn.and,
$$\mathrm{K}_{J,global} = k_J \begin{bmatrix} 1-\cos^2\alpha\sin^2\alpha & \cos\alpha\sin\alpha\sin^2\beta & -\cos\alpha\cos\beta\sin\beta \\ \cos\alpha\sin\alpha\sin^2\beta & 1-\sin^2\alpha\sin^2\beta & \sin\alpha\cos\beta\sin\beta \\ -\cos\alpha\cos\beta\sin\beta & \sin\alpha\cos\beta\sin\beta & \sin^2\beta \end{bmatrix}$$

(19) upon the onset of plasticity and it is a function of the plastic strain ε^{pl} and the stress σ. The handling of global intact rock conductivity tensor $\mathrm{K}_I^{(j)}\left(\varepsilon^{pl},\sigma\right)$ is similar to the global hydraulic conductivity tensor of joint sets, as depending on the mode of failure up to 3 additional virtual joint sets are introduced upon the onset of plasticity. In case of onset of shear failure the first two virtual joint sets of the intact rock are introduced along the two planes of maximum shear stress (at 45°). The third virtual joint set is introduced when the mode of failure is tensile and in the direction perpendicular to the maximum principle stress direction.

The update of the hydraulic conductivity of the joint set at the end of each calculation step is a function of the hydraulic joint opening e and the normal joint stress σ_N which simulates the closing of joint openings due to compressive normal joint stresses.

$$\mathrm{K}_J\left(e,\sigma_N\right)=\mathrm{K}_{J0}\left(e\right)f\left(\sigma_N\right) \tag{24}$$

The maximum value of the stress independent part of the hydraulic conductivity of the joint set K_{max} is a function of the maximum effective hydraulic opening e_{max} which is defined as an input parameter.

$$0 \le \mathrm{K}_{J0}\left(e\right) \le \mathrm{K}_{max} \tag{25}$$

To allow joint closure under compression stresses on joint surface a stress scaling function that simulates the effect of stress dependency decreases as a result of joint closure is uded. The function varies from 1 to 0 with increasing compressive normal joint stress and is 1 in case of tension.

$$0 \le f\left(\sigma_N\right) \le 1 \tag{26}$$

The value of hydraulic joint opening e is related to geometrical or the mechanical joint opening E by a user defined parameter *daGeomtoHydrOpeningRatio* which is the ratio of geometrical to hydraulic opening ratio with a variation window of between 1 and 2. The geometric opening is calculated from the normal joint plastic strain ε_N^{pl} and the joint set distance S as shown below.

$$E = \varepsilon_N^{pl} S \tag{27}$$

After the determination of hydraulic opening value e the stress independent hydraulic joint conductivity $\mathrm{K}_{J0}(e)$ is defined by the cubic law as follows.

$$K_{J0} = \frac{\gamma}{\mu} \frac{e^3}{12 S R_C} \text{ with } \left(0 \le e \le e_{\max}\right) \tag{28}$$

where,

γ – Specific weight of the fluid

μ – Dynamic viscosity of the fluid

e – Effective hydraulic joint opening

e_{max} – Maximum effective hydraulic joint opening

S – Joint distance

R_C – Joint roughness coefficient

The buildup of the joint hydraulic conductivity as a function of the hydraulic joint opening is illustrated in the fig.

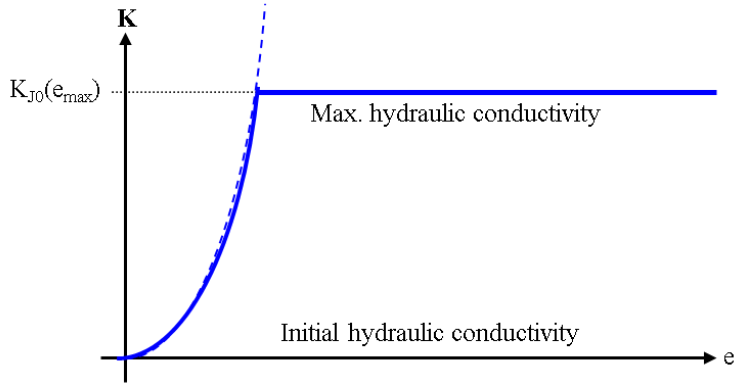

Fig. 9 Cubic law showing stress independent hydraulic conductivity as a function hydraulic joint opening.

The definition of stress dependency part is based on [7] and it is defined as follows

$$\mathrm{K}_J = \mathrm{K}_{J0} \begin{cases} 1 & \sigma_N > 0 \\ \left[1 - \overline{\mathrm{K}}_{min}\right] \left[1 - \left(\frac{\sigma_N}{D}\right)^{\frac{1}{n}}\right]^2 + \overline{\mathrm{K}}_{min} & D \le \sigma_N \le 0 \\ \overline{\mathrm{K}}_{min} & \sigma_N < 0 \end{cases} \tag{29}$$

where,

K_J – Hydraulic joint conductivity

K_{J0} – Hydraulic joint conductivity at $\sigma_N = 0$

$\overline{K}_{min}$ – Minimum hydraulic joint conductivity scaling factor

σ_N – Normal joint stress (It is negative in case of compressive stresses)

D – Limit joint normal stress

n – Shape parameter

The effect of stress dependency on the decay of hydraulic conductivity is depicted by the *Fig. 10* below.

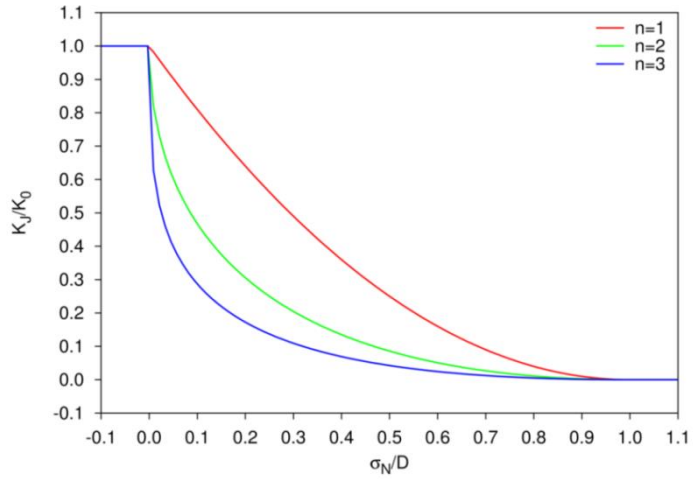

Fig. 10 Effect of stress dependency on the hydraulic conductivity.

2.4 Coupling of Hydraulic and Mechanical Meshes

It is important to note that in the coupling between hydraulic and mechanical domain we use for every mechanical discretization point one hydraulic finite element. Therefore in the discretization of the hydraulic fracturing simulator the so-called '1to8' approach is used. This means that 1 mechanical element is represented by 8 hydraulic elements as shown in the *Fig. 11*. The advantage of this coupling is that there is no averaging required for the fracture induced hydraulic conductivity calculated at the 8 integration points of a given mechanical element. Secondly this refinement of hydraulic mesh gives a much better representation of the pore pressure gradient in and near the plastic elements.

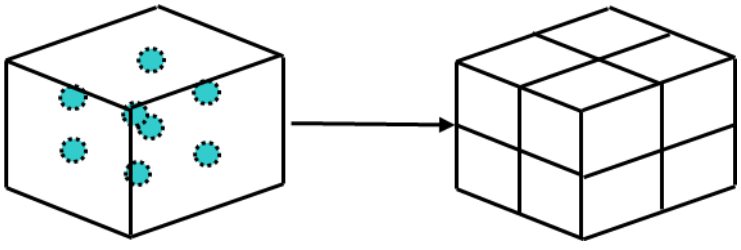

Fig. 11 Coupling of hydraulic and mechanical meshes.

2.5 Hydraulic to Mechanical Coupling

The fluid flow in joints results in pressure differences between joints and matrix rock which result in normal forces on the joint walls. Within the homogenized continuum approach these are called flow forces and their increments in a given calculation step depend on the pressure gradients in that step and they are also the input to next mechanical step that causes the rock deformation. This pressure gradient resulting from hydraulic height gradient results from the solution of the transient seepage equation in the hydraulic step. In the global directions the incremental flow force vector acting on a certain volume (body forces) is given by

$$\Delta J_i = -\Delta i_i . \gamma \tag{30}$$

where,

Δi_i – Increment of hydraulic height gradient

γ – Specific weight of the fluid

The final nodal force vector is obtained by integrating the body forces over the element volume. In the '1to8' approach the forces of one mechanical node is assembled from the total forces of all hydraulic elements which are connected to that node.

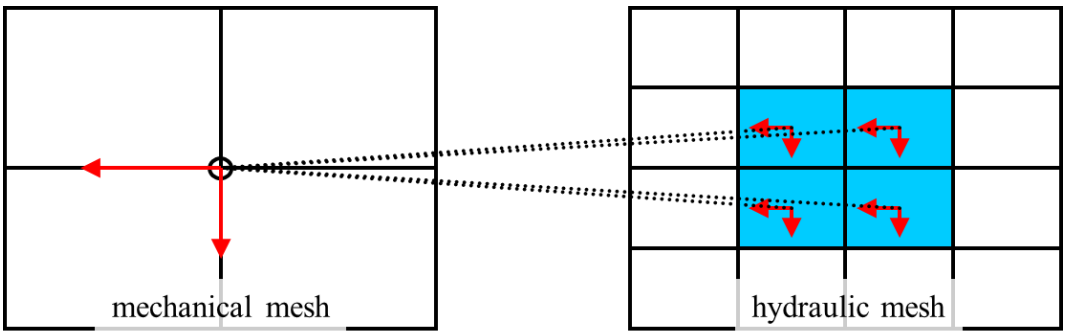

Fig. 12 Hydraulic-mechanical coupling of flow forces.

2.6 Initial conditions

The initial state in the hydraulic model is the initial pore pressure which are defined at top and bottom of every reservoir layer. Between the top and bottom of every layer a linear change of the pore pressure is assumed. At the interface between the layers the pore pressure values are averaged.

In the mechanical model for any activated or new joint the initial effective stresses are the initial conditions. Therefore the input to the simulator is the Terzaghi effective stresses in the initial mechanical model. The effective vertical stress values are defined as follows:

$$\sigma_{Vert,eff.} = \sigma_{Vert,total} - PP \tag{31}$$

where,

$\sigma_{Vert,eff}$ – Effective vertical stress

$\sigma_{Vert,total}$ – Total vertical stress

PP – Pore pressure

The minimum effective horizontal stress is related to the effective vertical stress by the k_0 value.

$$\sigma_{Horiz,min} = \sigma_{Vert,eff}.k_0 \tag{32}$$

where,

k_0 – Ratio between the effective vertical stress and minimum effective horizontal stress

$\sigma_{Horiz,min}$ – Minimum effective horizontal stress

Similarly, the maximum effective horizontal stress is defined in terms of minimum effective horizontal stress and the effective vertical stress.

$$\sigma_{Horiz,max} = \left(\sigma_{Vert,eff} - \sigma_{Horiz,min}\right).shmaxratio + \sigma_{Horiz,min} \tag{33}$$

where,

shmaxratio – The ratio of effective stress differences

$\sigma_{Horiz,max}$ – Maximum effective horizontal stress

The orientation of the effective stresses in the global coordinate system is controlled by the parameter *daIniStrMinHorizDir* which is the rotation of minimum horizontal stress about the global z-axis (along the True Vertical Depth (TVD)).

3 Modelling the Penny Shaped Frack

In this section the hydraulic fracturing simulator is applied to model the propagation of hydraulically driven fracture for the Penny shaped benchmark model, which is the horizontal,

circle-shaped, planar fracture within a cylindrical domain ([8], [9], [10]). The main goal of this exercise is to show the accuracy in prediction of the analytical result of benchmark model using the homogenized continuum approach for modelling of hydraulic fracturing.

This chapter starts with the explanation of fracture propagation regimes (as per [1]), followed by the model setup (geometry and mesh), initial, boundary conditions and loads in the model and finally the parameter calibration by performing the sensitivity and optimization studies.

3.1 Fracture Propagation Regimes

According to [1], during the hydraulic fracturing process there are two pairs of competing physical processes. The first pair consists of competing dissipative mechanisms: a) energy dissipated due to fluid viscosity and b) energy dissipated due to fracture propagation and the second pair consists of competing components of fluid balance: a) fluid storage within the fracture and b) fluid leakage from the fracture into the surrounding material. Depending on which of the two dissipative mechanisms and which of the two storage mechanisms dominate, four primary limiting regimes of propagation emerge:

- Viscosity and storage dominated propagation regime (M).
- Toughness and storage dominated propagation regime (K).
- Viscosity and leak off dominated regime $(\tilde{M})$.
- Toughness and leak off dominated regime $(\tilde{K})$.

The publication [1] shows that these four fracture propagation regimes can be conceptualized into a rectangular parametric space where each regime corresponds to each vertex of the rectangle. Out of the four propagation regimes only the toughness and storage dominated propagation regime (K) and the viscosity and storage dominated propagation regime (M) were probed in the study by [1]. For the current study only the K -vertex will be investigated as it is the most relevant propagation regime for the hydraulic fracturing process in unconventional reservoirs.

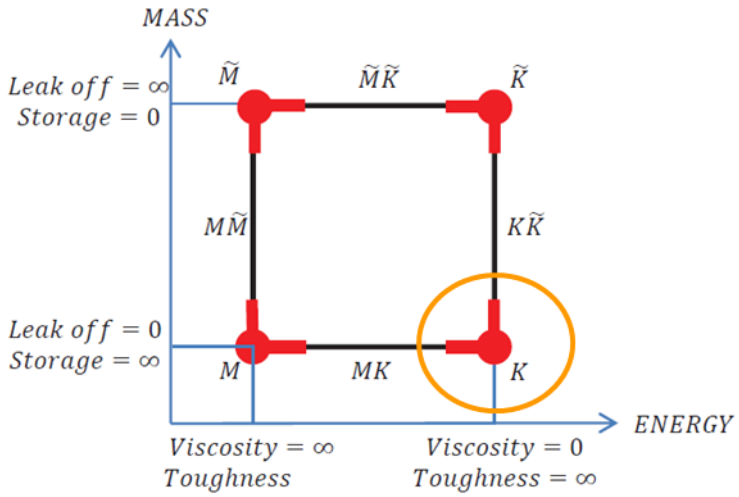

Fig. 13 The four limiting propagation regimes of the hydraulic fracturing process [1], *with* K *-vertex being most relevant to current study.*

3.2 The Benchmark Model Description

The form and dimensions of this benchmark model is based on the ([1]) study. It is an axisymmetric, penny shaped, hydraulically driven fracture propagating in a cylindrically shaped saturated low permeable medium. The model dimensions are characterized by the inner radius R_0, outer radius R_1 and the height H. The saturated low permeable medium is characterized by the elastic parameters, Young's Modulus E and Poisson's ratio ν, the joint strength parameters, the tensile strength at yield σ_t and residual strength σ_{tr}, the initial permeability of the medium/rock matrix k_{ini} and initial confinement stress σ_0 if any in the model. An incompressible Newtonian fluid with viscosity of μ_f is injected at a constant rate of Q_0 at the center of the fracture from the vertical wellbore. For the given input parameters the fracture aperture or joint opening $w(r,t)$ as a function of fracture radius r, time t, the net pressure $p(r,t)$ as a function of radius r, time t and the fracture extension $R(t)$ as a function of time t are the desired responses.

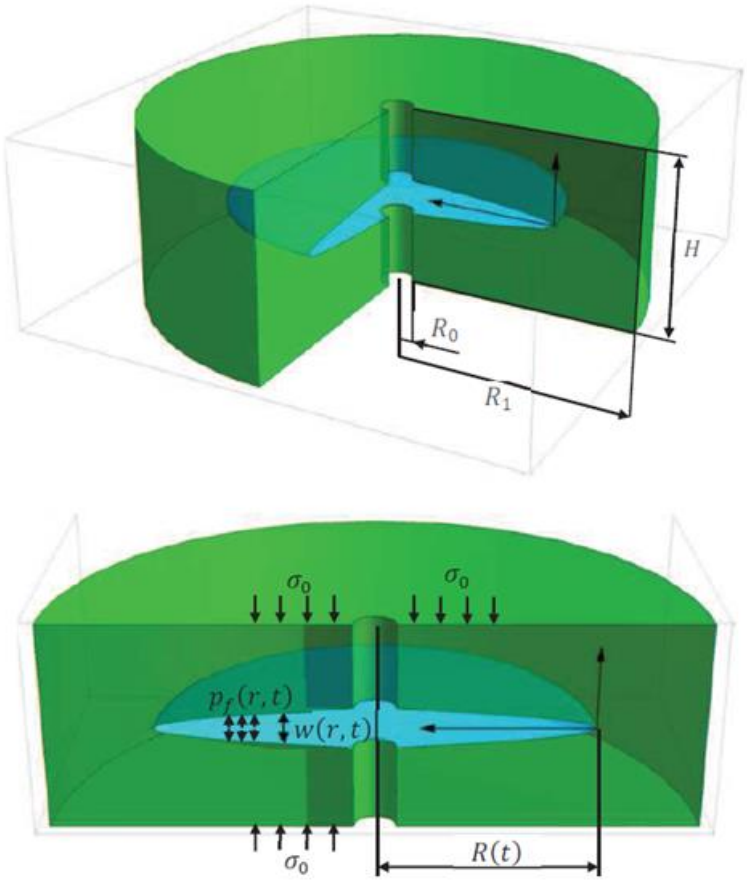

Fig. 14 The cylindrical domain showing the horizontal, penny-shaped, hydraulically driven fracture [1].

3.3 Model geometry and mesh

A 3-D finite element model is investigated in this study. Due to axial symmetry of the problem only one quarter of the model 3D domain is considered. Another difference to be noted is that unlike the cylindrical geometry in the previous section, the model geometry as generated by the Dynardo simulator is cuboidal, but this does not have any influence on the results as the model is made large enough to avoid or minimize the boundary effects. The model dimensions and the mesh definitions are defined as per the values in the table from [1].

Dimension	**Value**
Inner radius	$R_0 = 0.01m$
Outer radius	$R_1 = 45m$
Height	$H = 30m$
Angle	$\theta = 90°$

Table 1 Penny shaped model dimensions from [1].

The *Fig. 15* shows the mesh of the mechanical model. The structural domain is discretized with eight node structural SOLID185 elements. Representing a comparable discretization level like [1] the total number of elements in the model are 27 216. The *Fig. 16* depicts the top view of the model with mesh and the volume which distinguishes the coarse and fine mesh regions. The element lengths in the fine and coarse mesh regions are 0.5 m and 4.0 m respectively. The fine mesh region is assumed to be large enough to cover the fracture extension of the analytical results in [1]. To define the location of the inflow we define a "perforation" element.

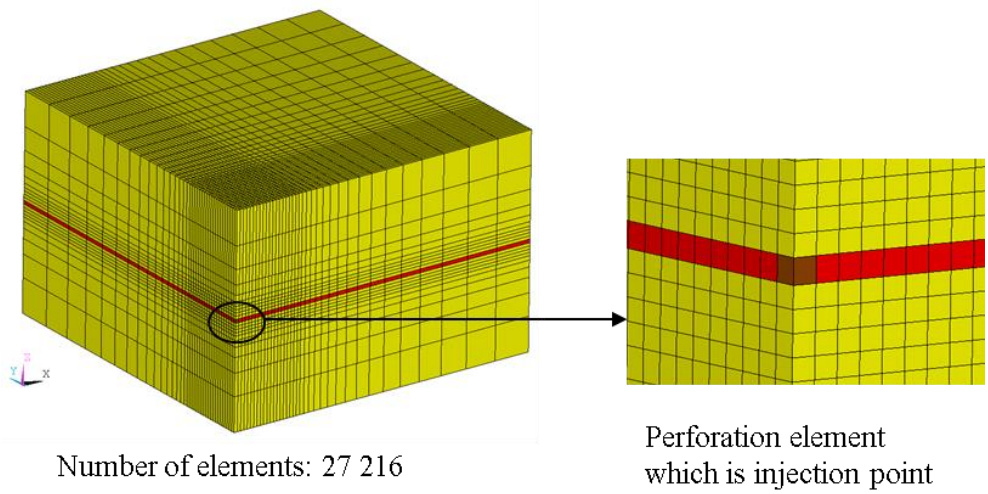

Fig. 15 The isometric view of the mechanical model along with the zoomed view showing the point of injection or the perforation element.

The transverse view of the model depicts the layering in the model. The topmost and bottommost layers of the model, Elastic_1 and Elastic_2 have only elastic material properties The failure mode of the theoretical solution is a tensile failure in the middle layer, therefore that layer is modelled with plastic behavior to have planar tensile strength anisotropy. The tensile strength mode is defined with initial tensile strength and post yield (residual strength properties). The fluid is injected at the perforation element. The height and horizontal length of the perforation element is 0.5 m. The element sizes in fine and coarse mesh regions in the transverse direction are 0.5 m and 4.0 m respectively. The fine mesh volume region is made larger than the plastic region to avoid the sudden transition of the mesh size directly at the interface of the two layers.

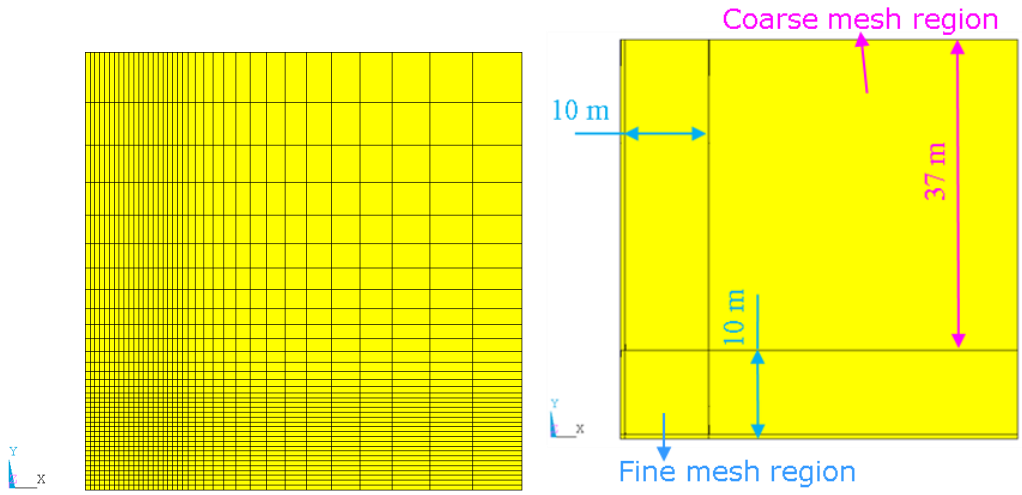

a) b)

Fig. 16 a) Mesh top view b) Volume plot depicting the coarse and fine element regions

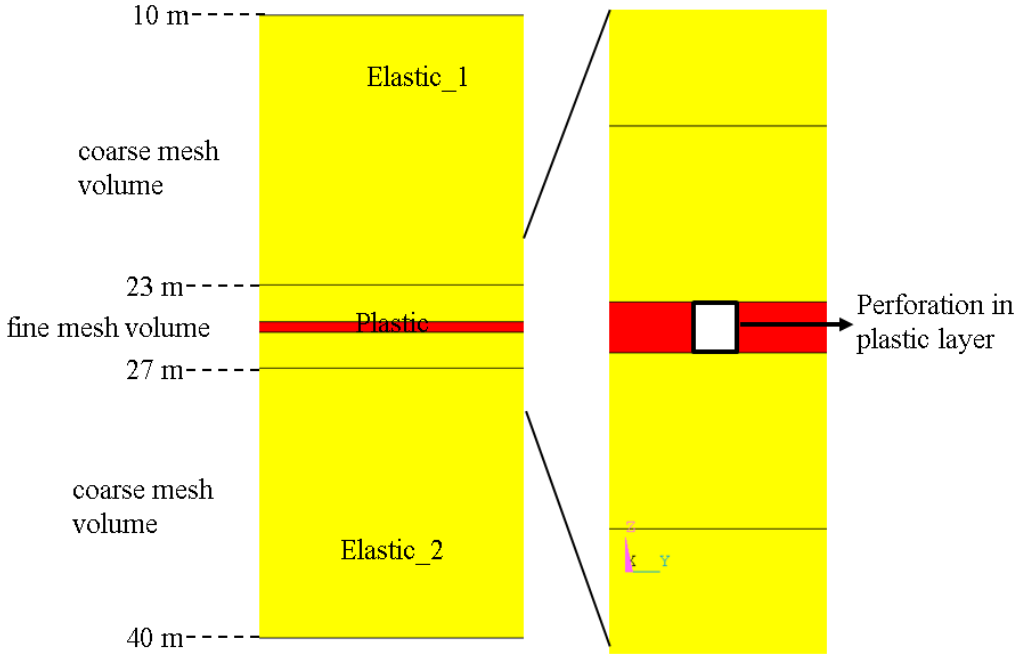

Fig. 17 The transverse view showing the layers

Layer name	Top [m]	Bottom [m]	Thickness [m]
Elastic_1	10.00	24.75	14.75
Plastic	24.75	25.25	0.50
Elastic_2	25.25	40.00	14.75

Table 2 The layering and layer dimensions of the model

Due to 1:8 mesh coupling of mechanical and hydraulic models the number of elements in hydraulic model is eight times that of the mechanical model with 2 17 730.

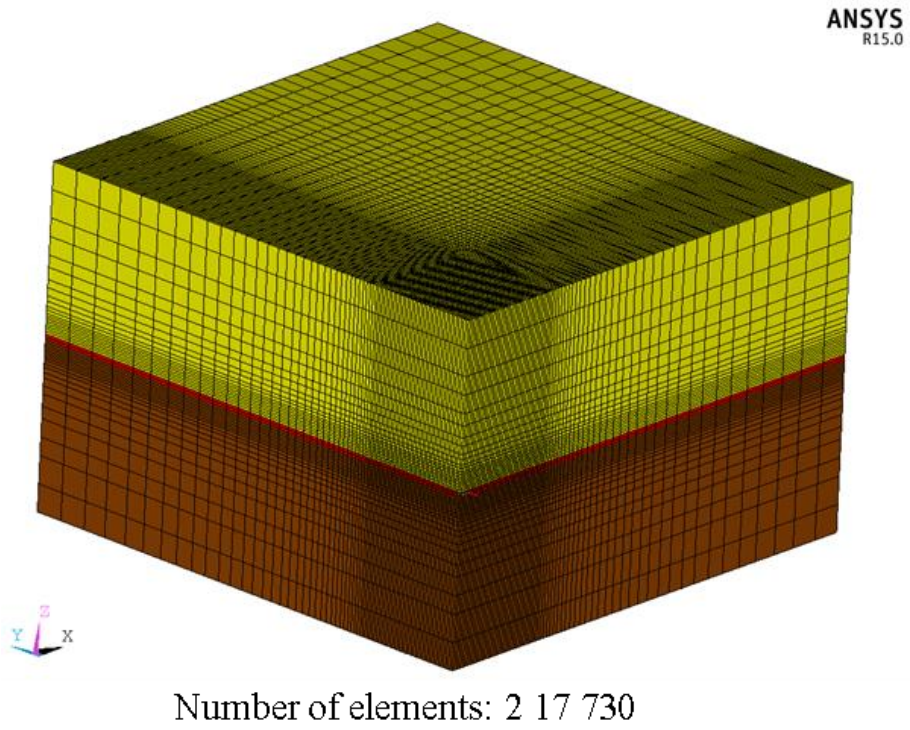

Fig. 18 The isometric view of the hydraulic model

3.4 Initial Conditions, Boundary Conditions and Loads

The initial and boundary conditions are applied to both the mechanical and the hydraulic models. In the mechanical model all the displacement degrees of freedom on the nodes on the external faces are fixed. On the nodes on the symmetry faces of the model the displacement DOF perpendicular to that face is fixed. . Based on the [1] there are no initial effective stress in the mechanical model.

In the hydraulic model, no flux condition is applied on the symmetry faces. According to [1] there is no initial pores pressure or hydraulic head in the model and the fracturing fluid is injected at a constant rate of 0.001 m^3/s for 40 s. In Dynardo fracturing simulator since a quarter symmetry model is considered, an injection rate of 0.001/4 m^3/s is applied to the perforation element for 40 s.

Initial conditions		
Initial fluid pore pressure	p_0	0.0
Initial principle in situ stresses	$(\sigma_1^0, \sigma_2^0, \sigma_3^0)$	(0.0,0.0,0.0)

Table 3 The initial state of the model based on [1].

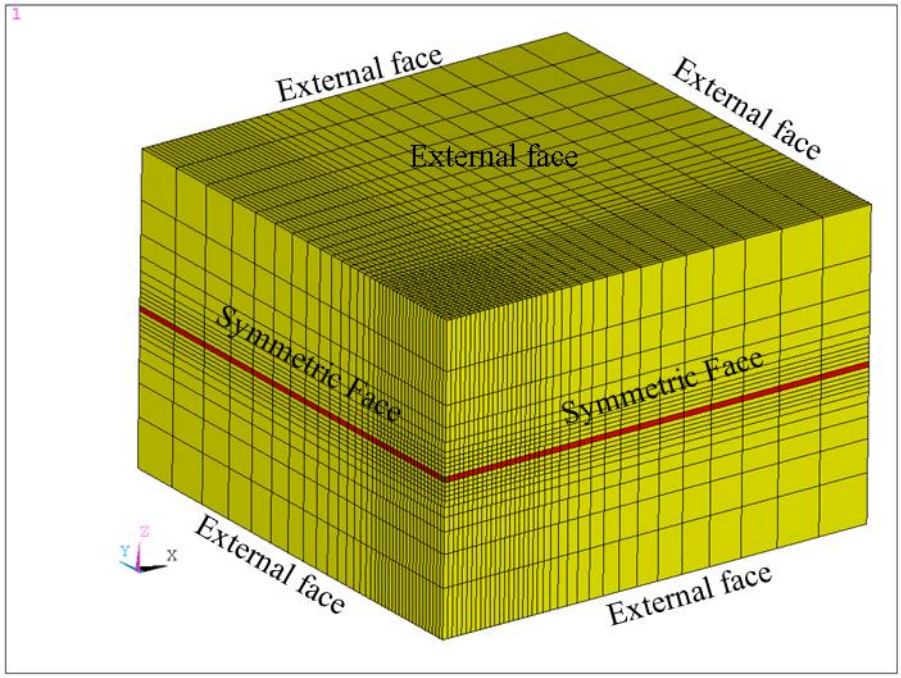

Fig. 19 The isometric view of the mechanical model showing the symmetric and external faces.

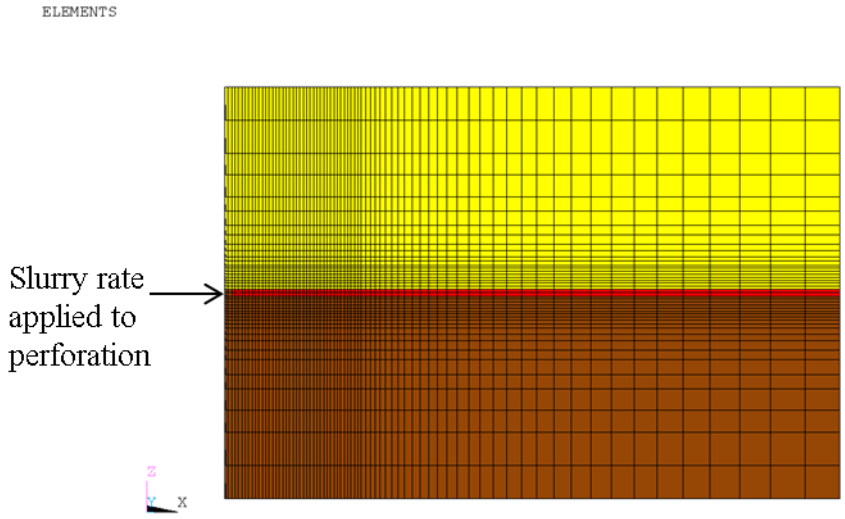

Fig. 20 The side view of hydraulic model showing the slurry rate applied to the perforation element.

3.5 Material Parameters

As it is discussed earlier the investigated material law for jointed rocks in Dynardo simulator assumes a brittle tensile failure behavior and post-yield the material strength values are reduced to the residual strength values. The material law considered in the [1] on the other

hand assumes a post-yield linear softening behavior with a fracture energy value. Hence an one to one translation of the material parameters from [1] initially are not expected to produce a perfect agreement with the analytical results. The necessary calibration of the parameter of the brittle material low to match an energy based softening law was solved by performing a sensitivity study to establish a relationship between the strength parameters and important results like the pressure and joint opening. Having that relationship identified a calibration is performed to find the strength parameters which consequently resulted in a good match with the analytical results. This section proceeds with describing the initial parameter set obtained directly from the [1] paper, then the parameter calibration study that are performed to fit the parameters.

3.5.1 Mechanical and Hydraulic Parameters

The isotropic linear elastic material properties in all the three layers are taken directly from the [1] as listed in the *Table 4*. The shear modulus G is calculated from the Young's modulus E and the Poisson's ratio ν.

$$G = \frac{E}{2(1+\nu)} \tag{34}$$

Parameters	**Value**	**Unit**
Young's modulus (E)	17.00	[GPa]
Poisson's ratio (ν)	0.20	[GPa]
Shear modulus (G)	7.08	[-]

Table 4 The elastic properties based on [1].

The middle plastic layer of the model is initialized with rock matrix or intact rock along with one horizontal plane of weakness or the bedding plane with dip angles of 0°/0°. The intact rock failure is disabled by defining random high strength values for it and only the bedding plane failure is enabled to induce horizontal pancake fracture growth in that layer. The shear failure of the bedding plane is also disabled by defining high shear strength value for the bedding plane. Only the tensile failure of the bedding plane is enabled and the cohesive strength value of 1.25 MPa from [1] is assumed as the initially as tensile strength of the bedding plane. The initial value of residual tensile strength is set at a very low value of 0.1% of the initial.

Initial definition of strength parameters		
Parameters	**Value**	**Unit**
Tensile strength (σ_t)	1.25	[MPa]
Residual tensile strength factor (σ_{t_res})	0.001	[-]

Table 5 The bedding plane strength parameters based on [1].

It needs to be noted that within the homogenized continuum approach the plastic strain needs to be converted into a joint opening by assuming a frequency of joints using the parameter joint distance. To model one single fracture in the bedding plane, the joint distance S in the plastic layer is assumed to be very large (10 m) which is much higher than the element length of 0.5 m in the fine mesh region. Translating of the theoretical solution, the joint roughness coefficient JRC is set 1 which signifies that the fracture planes are perfect. The fracturing fluid is modelled as Newtonian fluid with viscosity μ of 0.1 cP for the toughness and storage dominated regime or K-vertex in the *Fig. 13* as per [1]**.** Since there is no leak off in the model, the isotropic initial permeability k_{ini} of the rock matrix is assumed to have a very low value of 1e-24 m^2. To match the theoretical solution, the parameter geometric to effective hydraulic opening ratio E/e is assumed to be 1.0 to neglect its effect in the calculation of hydraulic effective joint opening. Similarly the maximum effective hydraulic opening is set a high value to negate its influence on the hydraulic conductivity build up in the model. The effect of compressive stresses or the stress dependency part of the hydraulic conductivity is also switched off due to its irrelevance for the simple benchmark models like the penny shaped frack model. As it is mentioned earlier the specific storativity or specific storage is a physical property that characterizes the capacity of an joint to release the fluid and thereby sustains the volume balance between the mechanical joint opening and related hydraulic fluid consumption i.e. to maintain sameness between the amount of fracturing fluid pumped in the system and the resulting fracture or joint volume. This parameter is usually calibrated for any given discretization level to achieve volume balance at the end of pumping of the stipulated amount of fracturing fluid in the system in a low permeable environment with negligible leak off. These aforementioned parameters are tabulated below (*Table 6*).

Parameters	Value	Unit
Joint distance (S)	10.00 (changes to equivalent element length)	[m]
Joint roughness Coefficient (JRC)	1.00	[-]
Fluid viscosity (μ)	0.10	[cP]
Isotropic initial permeability (k_{ini})	1.00E-24	[m^2]
Geometric to hydraulic opening ratio (E/e)	1.00	[-]
Maximum effective hydraulic opening (e_{max})	1.00 (very high value to nullify it)	[m]

Table 6 The hydraulic parameters in Dynardo fracturing simulator.

3.5.2 Parameter Calibration

With the initial assumed parameter of the brittle tensile failure it was observed that the pressure and joint opening values are underestimated. This can simply be attributed to the brittle nature of the material model (with very low residual strength value) used in Dynardo fracturing simulator. It was inferred from the initial findings that the strength parameters i.e. tensile strength and residual tensile strength are the two relevant parameters for further investigation. To confirm this, a test simulation was performed with higher value of tensile strength of 2.5 MPa with a low residual tensile strength value of 0.1% of the initial value which as expected resulted in overestimation of the opening and the pressure values.

At this point is should be noted that the Dynardo simulator provides energy based material models, but for simplicity and practical relevance we want to show how we calibrate a simple fracture model to fit the available theoretical solutions. That task we regularly have to perform for real world hydraulic fracturing simulations to a large number of uncertain parameter which needs to be calibrated to best available measurement data. Therefore here we demonstrate the process for the simple problem to calibrate two strength values.

Based on the initial simulations it was clear that the value of strength parameters should be in between the initial values and the overestimated higher strength values. To assess the

influence of strength parameters towards the outputs, pressure and fracture opening, a sensitivity study was performed followed by a calibration step to fit the strength parameter. For both the sensitivity and the calibration step the Dynardo software optiSLang was used. The variation window of the uncertain strength parameters, the tensile strength $M2\_sigt\_1$ and residual tensile strength factor of initial value $M2\_sigtr\_1$ was assumed to.

Parameters	**Parameter names**	**Reference**	**Range**	**Unit**
Tensile strength	$M2\_sigt\_1$	1.25	[1.00-2.50]	[MPa]
Residual strength factor	$M2\_sigtr\_1$	0.001	[0.001-0.200]	[-]

Table 7 The variation window of the tensile strength and the residual tensile strength factor for the sensitivity study.

Within parameter bounds the Advanced Latin Hypercube sampling (ALHS) was used to generate a set of possible Parameter combinations. Here a sample size of 61 design points was used in the sensitivity study. For the simple two dimensional problem, the approach to start with a sensitivity analysis based on ALHS sampling and the ability to automatically reduce the number of important parameter is not effective, but that approach scales without too much additional support points up to multiple hundred parameters [11] and is here shown for demonstration purpose. Note that the Dynardo sensitivity approach usually assumes a large number of uncertain parameter and assumes as a first step, that the important parameter to calibrate needs to be identified by an scan of the design space followed by an global sensitivity measure which is Coefficient of Prognosis (CoP) value using the Metamodel of Optimal Prognosis (MOP) approach.

The responses that were evaluated for the sensitivity study were as follows:

- $diff\_Jntopn\_perf\_EOP$*:* Magnitude of difference between the simulation and analytical value of joint opening in the perforation element (near the injection point) at the end of pumping (*Fig. 21*).
- $diff\_press\_perf\_EOP$*:* Magnitude of difference between the simulation and analytical value of the pressure in the perforation element (near the injection point) at the end of pumping (*Fig. 22*).

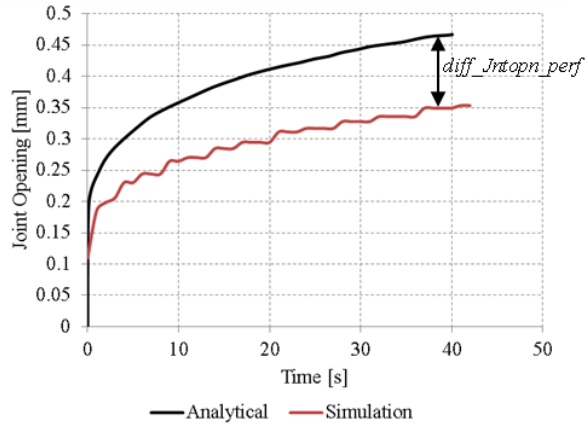

Fig. 21 Joint opening plot near the injection point showing the response, $diff\_Jntopn\_perf\_EOP$.

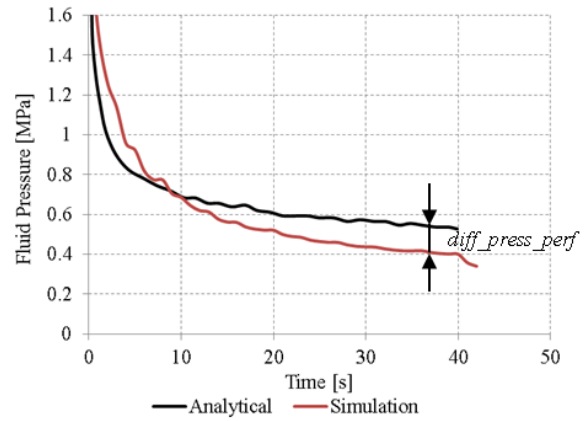

Fig. 22 Pressure near the injection point showing the response, $diff\_press\_perf\_EOP$.

The *Fig. 23* shows the optiSLang result for the first response, $diff\_Jntopn\_perf\_EOP$ from the sensitivity study. The *Fig. 23* depicts that out of the two parameters considered in the sensitivity study only the tensile strength $M2\_sigt\_1$ has an influence on the response determining the joint opening with CoP-value of 96% which indicates a very good forecast quality to the response variation based on the MOP.

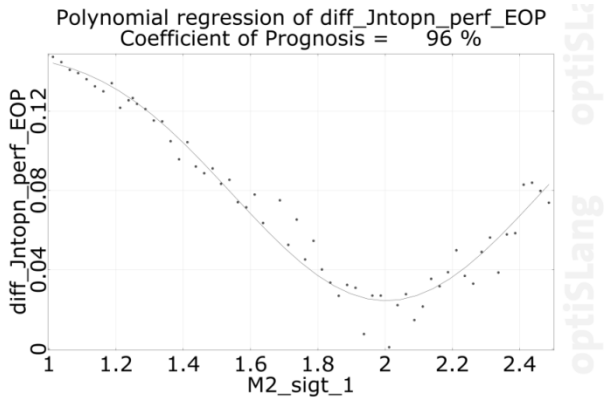

a)

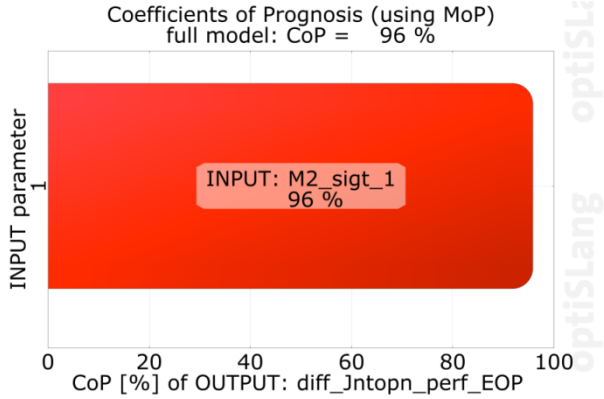

b)

Fig. 23 Response surface (MOP) and Coefficient of Prognosis (CoP) of the response, $diff\_Jntopn\_perf\_EOP$.

The results of second response, $diff\_press\_perf\_EOP$ (*Fig. 24*) show that both parameter, the tensile strength $M2\_sigt\_1$ and the residual tensile strength $M2\_sigtr\_1$ are significant. This response has a high CoP at 97% and therefore the MOP result again a very good predictability of the response variation.

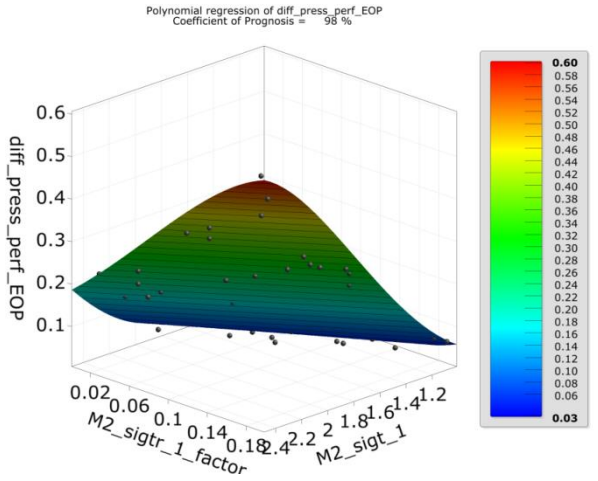

a)

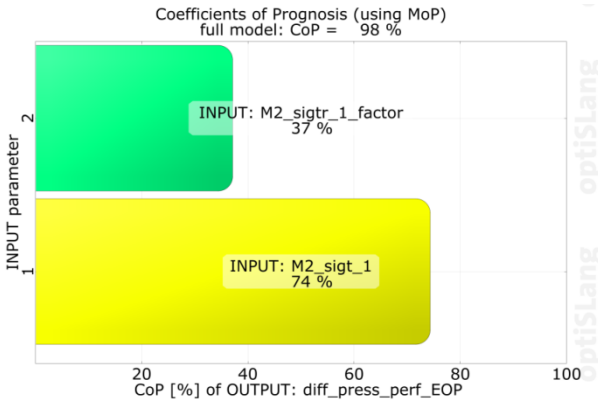

b)

Fig. 24 Response surface (MOP) and Coefficient of Prognosis (CoP) of the response, diff _ press _ perf _ EOP .

It can be validated from CoP values that there is a very good predictability of the variation of the responses with respect to the variation of the two important input parameters using the identified MOP's. A single objective function is defined which is the combination of the two responses from the sensitivity study each with a weightage of 50%. The goal of the optimization is to minimize this objective function and in this study the evolutionary algorithm of optiSLang is used for calibration purpose. The *Fig. 25* shows the best design from the optimization study and the corresponding values of the responses predicted based on the MOP's generated by optiSLang. The results obtained based on these best fit design input parameters are documented in the next section.

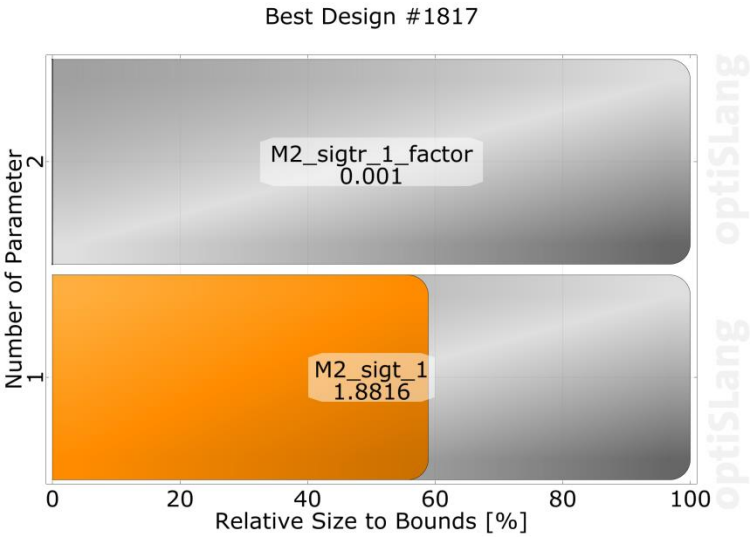

a)

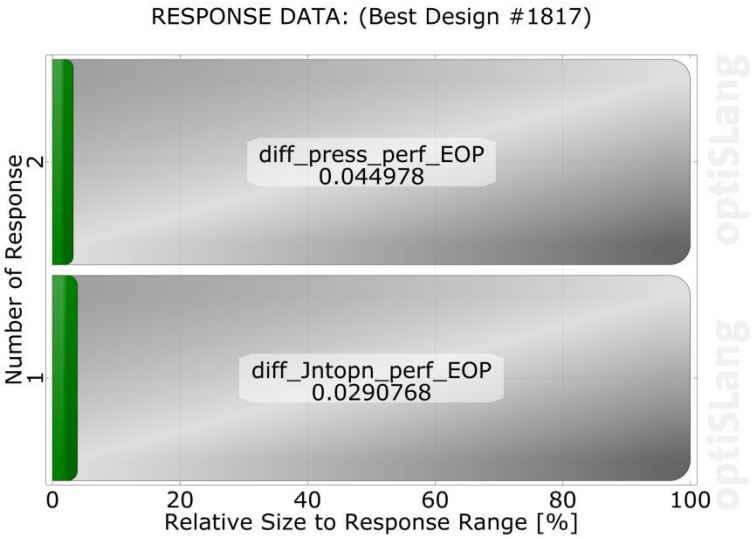

b)

Fig. 25 a) The best fit design input parameters based on the optimization study, b) the corresponding response values predicted by the optiSLang.

Best fit design strength parameters		
Parameters	**Value**	**Unit**
Tensile strength (σ_t)	1.88	[MPa]
Residual tensile strength factor (σ_{t_res})	0.001	[-]

Table 8 The best design strength values obtained from the optimization study.

4 Results

The final results based on the calibrated strength parameters are documented and discussed in this section for the toughness and storage dominated propagation regime (K-vertex). *Fig. 26*, *Fig. 27*, *Fig. 28* and *Fig. 29* display the variation of fluid pressure near the injection point in time, joint opening in time, fracturing fluid pressure distribution and joint opening along the crack evaluated at the end of pumping. In all the figures below the simulation results have been compared to the asymptotic analytical solution and there is very good agreement.

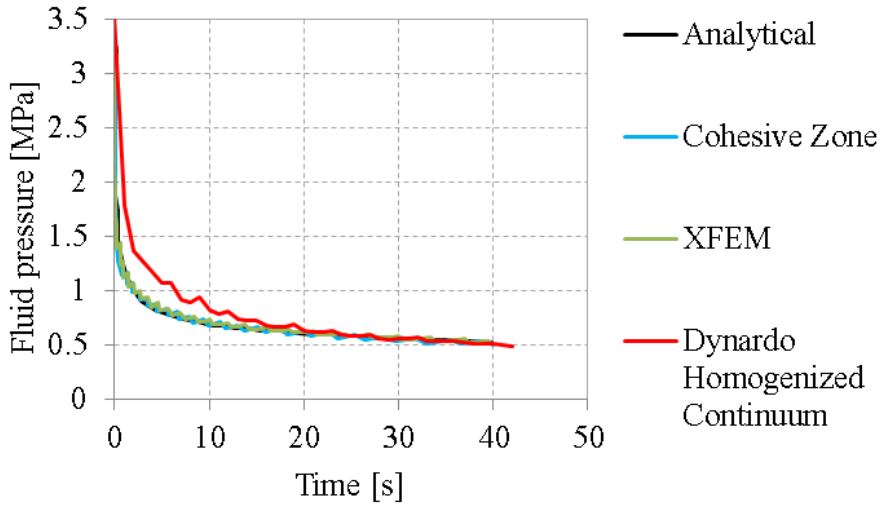

Fig. 26 Time evolution of the fluid pressure near the injection point.

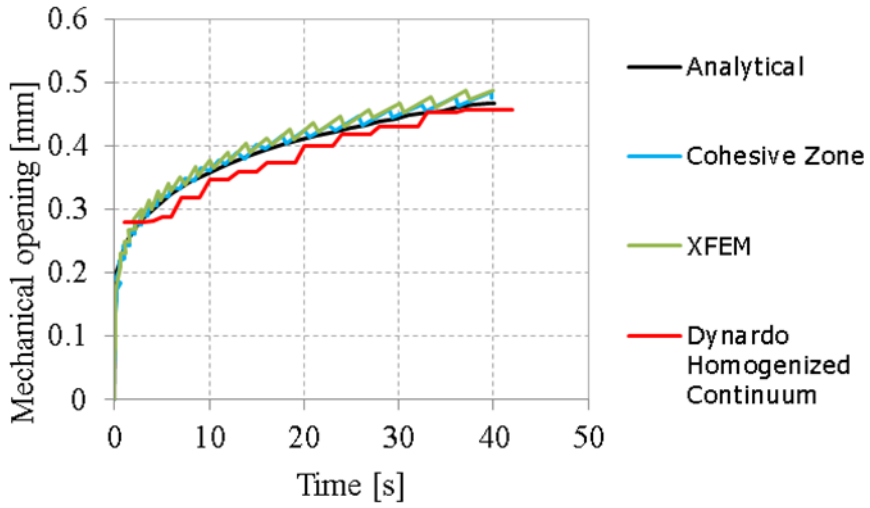

Fig. 27 Time evolution of joint opening near the injection point.

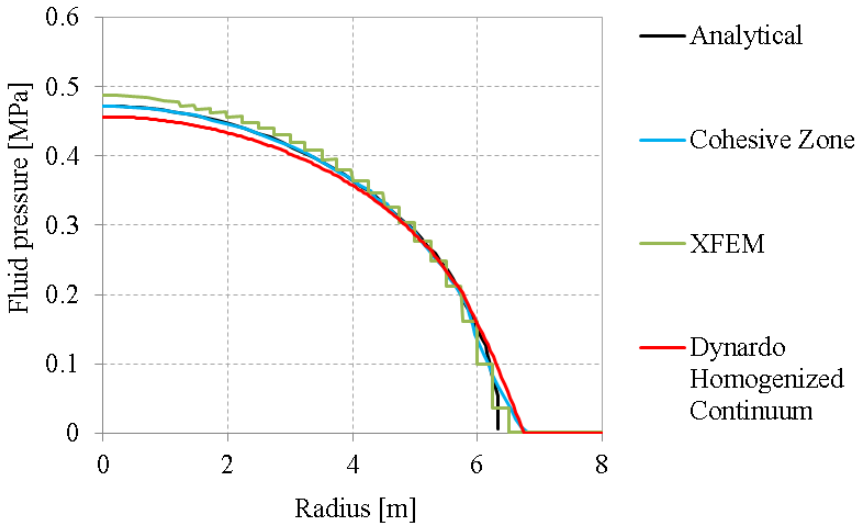

Fig. 28 Joint opening along the crack at the end of pumping.

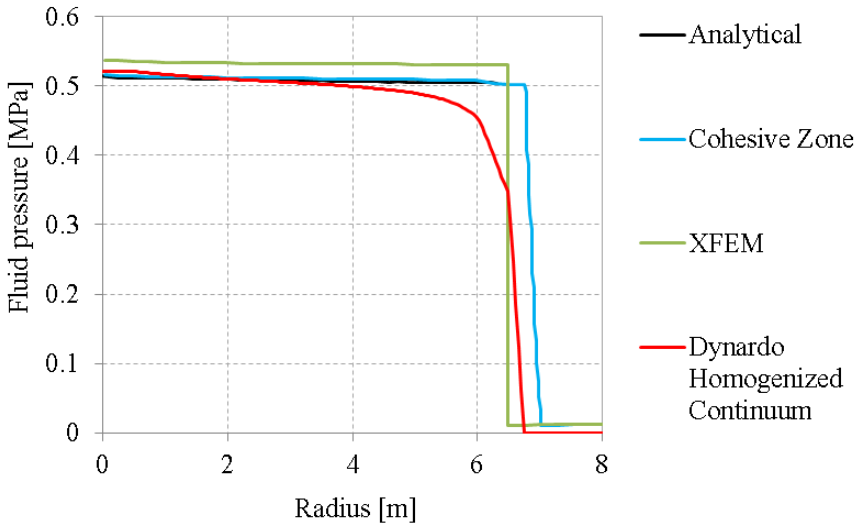

Fig. 29 Fluid pressure along the crack at the end of pumping.

The *Fig. 30*, *Fig. 31* and *Fig. 32* below are the contour plots showing the mapped and transverse views of pressure, joint conductivity and joint opening at the end of pumping which are few post processing outputs of Dynardo fracturing simulator.

In [1] there are contour plots of the maximum principle effective stress at the end of pumping for cohesive element method and the XFEM approaches. The comparisons with the plots generated from Dynardo fracturing simulator show a good match.

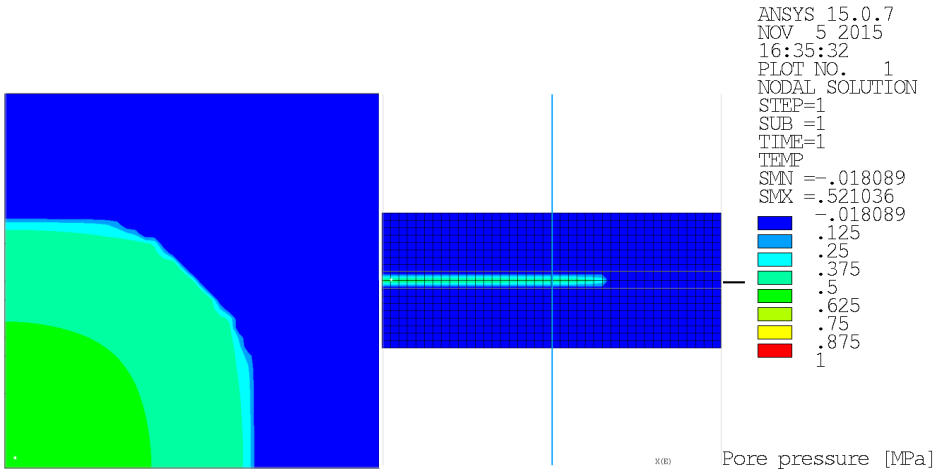

Fig. 30 Contour plot of the fluid pressure along the crack at the end of pumping.

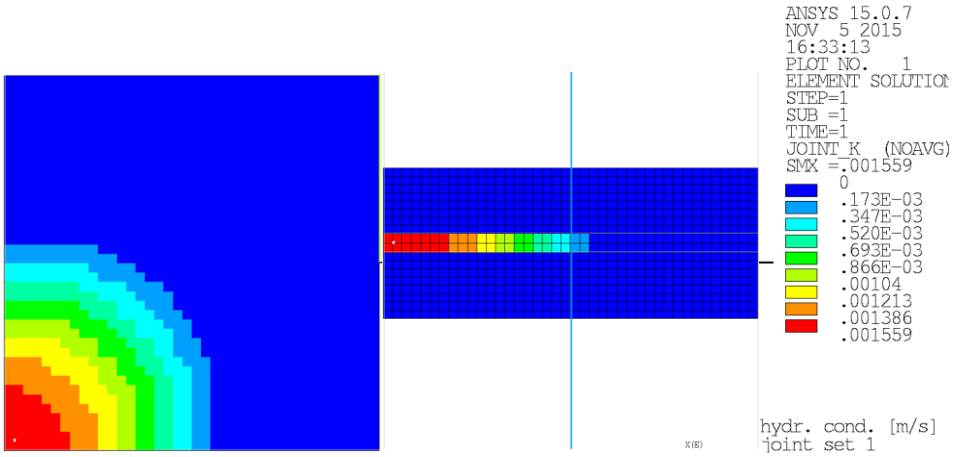

Fig. 31 Contour plot of the hydraulic conductivity along the crack at the end of pumping.

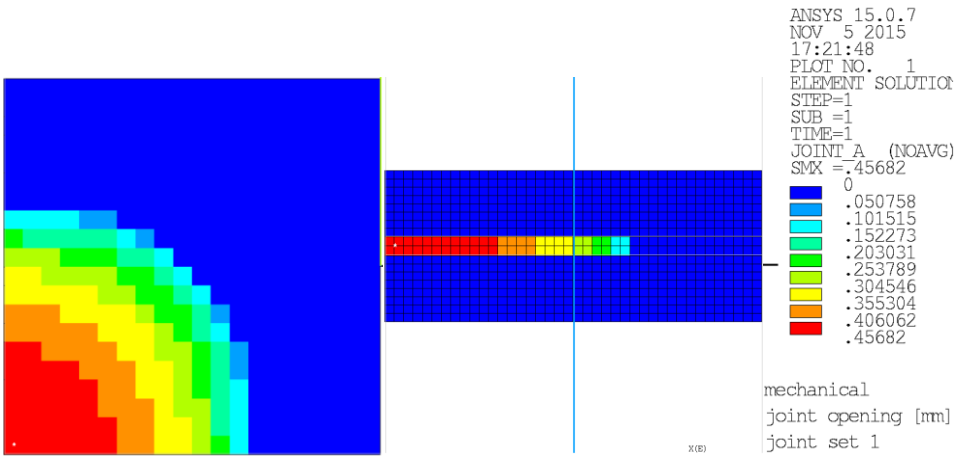

Fig. 32 Contour plot of the joint opening along the crack at the end of pumping.

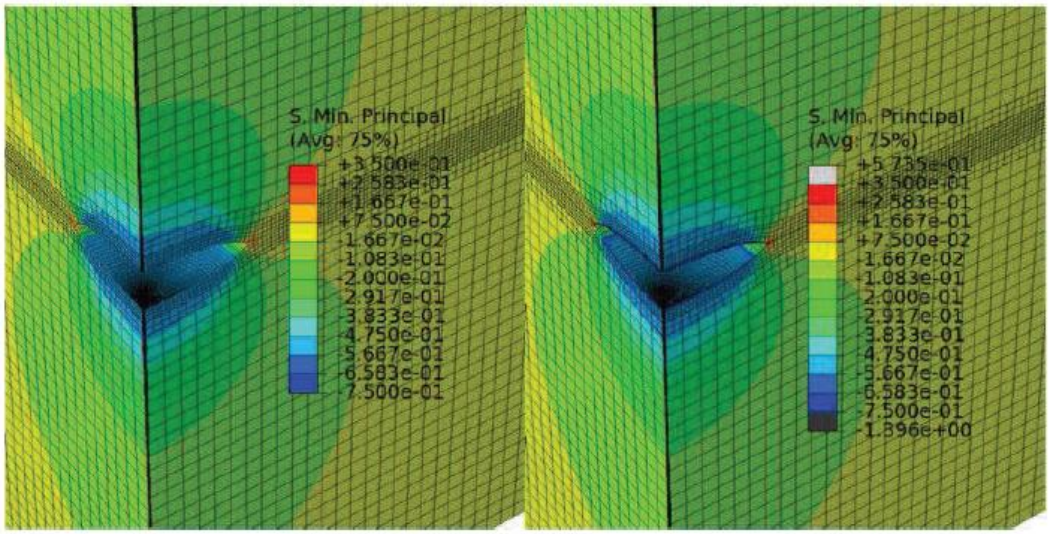

a)

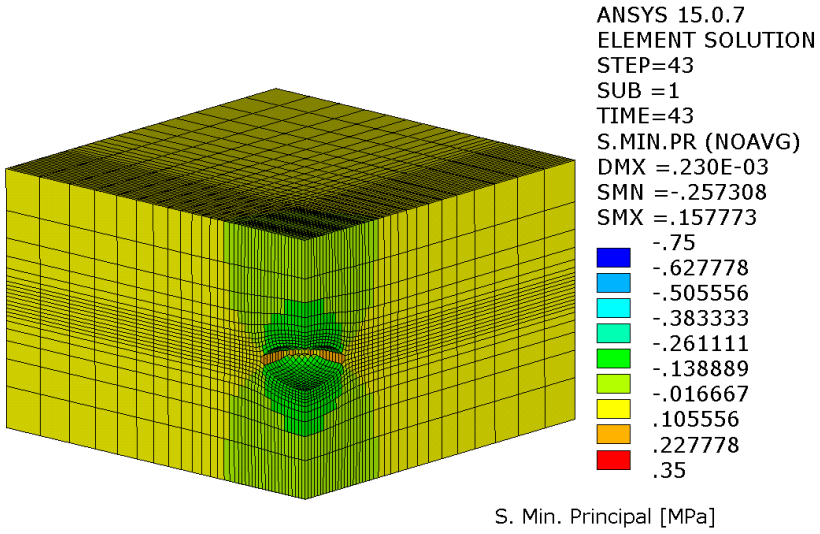

b)

Fig. 33 Maximum effective principal stress for models based on a) Cohesive element method (left), XFEM method (right) in [1] *and b) Dynardo fracturing simulator*

5 Conclusion and Outlook

In this paper it was shown that the homogenized continuum approach along with the discrete joint modelling solution using cohesive zone modelling in continuum mechanics or XFEM approach in continuum mechanics [1] each show good agreement with the analytical solution of the penny shaped fracture in saturated low permeable medium.

From here on the right approach to be followed for the industrial applications of hydraulic fracturing will be discussed. The discrete modelling of fracture using cohesive zone elements or any other predefinition of the fracture geometry are good enough to produce post processing verification pictures after the fracture network orientation and extension are known, but such modelling approaches cannot be used for the prediction of how the different well position or different stimulation procedure will affect fracture network growth. The alternatives to predefinition of fracture location which can be used for the prediction of fracture growth network are either XFEM, particle discretization or homogenized continuum approach. But the strategies of discrete modelling of fracture growth in 3D with the possibility of modelling different fracture systems under different operational conditions using XFEM or Particle code modelling are numerically extremely expensive and applying such strategies for reservoir modelling with multiple stages and multiple wells are not to be foreseeable within next decades.

On the other hand, in the homogenized continuum approach the element sizes can be reasonably large which result in reasonable CPU requirements, while still producing major phenomena of hydraulic fracturing like stimulation of multiple fracture sets, the network orientation, extension and their influence on resulting hydrocarbon production [3]. Of course the forecast quality of the most important physical phenomena for any given finite element discretization level, which drive the fracture network generation and the resulting hydrocarbon production out of the fracture network needs to be shown and verified. But in any case a calibration process of a reservoir model due to the numerous number of uncertain reservoir pressure, stress and strength parameters is necessary and therefore the calibration of a few “discretization” dependent parameters of the homogenized continuum approach like storativity and activated joint distance is not adding significant complexity or uncertainty to the overall process [3].

Therefore the homogenized continuum approach today seems to be the only approach available, which can be used to optimize stimulation procedure of unconventional oil and gas reservoirs at reservoir level modelling single or multiple wells using numerical simulation.

6 References

[1] M. G. Zielonka, K. H. Searles, J. Ning and S. R. Buechler, "Development and Validation of Fully-Coupled Hydraulic Fracturing Simulation Capabilities," in *2014 Simulia Community Conference*, 2014.

[2] L. Weijers, "Evaluation of Oil Industry Stimulation Practices for Engineered Geothermal Systems," Pinnacle Report DOE-PS36-04GO94001, October 2007.

[3] J. Will and T. Bai, "Hydraulic Fracturing Modelling Workflow and Toolkits for Well Completion Optimization of Unconventionals," in *Proceedings ANSYS Convergence Conference*, Houston, 2015.

[4] W. Wittke, Rock mechanics: theory and applications with case histories, The University of California: Springer, 1990, ISBN: 0387527192, 9780387527192.

[5] R. Schlegel, J. Will and M. Jobmann, "Using Statistical Methods for Rock Parameter Identification to analyse the THM Behaviour of Callovo-Oxfordian Claystone," in *Second EAGE Workshop on Geomechanics and Energy*, Celle, 13-15 October 2015.

[6] Dynardo GmbH, Dynamic Software and Engineering GmbH, "multiPlas- Elastoplastic material models for Ansys," Weimar, October 2014.

[7] A. Gangi, "Variation of whole and fractured porous rock permeability with confining pressure," *Int. J. Rock Meeh. Min. Sci. Geomeck. Abstr*, pp. 249-257, 1978.

[8] M. P. Clearly, "Comprehensive Design Formulae for Hydraulic Fracturing," *Society of Petroleum Engineers SPE-9259-MS*, 1980.

[9] P. A. Charlez, "Rock Mechanics, Volume 2, Petroleum Applications," *Editions Technip*, 1997.

[10] C. H. Yew, "Mechanics of Hydraulic Fracturing," *Gulf Publishing Company, Houston, TX*, 1997.

[11] T. Most and J. Will, "Efficient sensitvity analysis for virtual prototyping," in *Proceedings of the 6th European Congress of Computational Methods in Applied Sciences and Engineering*, Vienna, 2012.